A High Angle of Attack Inviscid Shuttle Orbiter Computation

William L. Kleb*

and

K. James Weilmuenster†

NASA Langley Research Center, Hampton, Virginia, 23665

Abstract

As a preliminary step toward predicting the leeside thermal environment for winged reentry vehicles at flight conditions, a computational solution for the flow about the Shuttle Orbiter at wind tunnel conditions was made using a point-implicit, finite volume scheme known as the Langley Aerothermodynamic Upwind Relaxation Algorithm (LAURA). The Scheme is a second-order accurate, upwind-biased Navier-Stokes solver capable of solving non-equilibrium chemistry flows with radiative equilibrium wall temperatures and finite-rate wall catalysis. For this study, however, the code is run in its simplest form, *i.e.*, inviscid flow using perfect gas chemistry. The surface pressures resulting from the computational solution are compared with wind tunnel data. The results indicate that the dominant inviscid flow features are being accurately predicted on the leeside of the Shuttle Orbiter at a moderately high angle of attack.

---

*Research Engineer, Aerothermodynamics Branch, Space Systems Division.

†Senior Research Engineer, Aerothermodynamics Branch, Space Systems Division.

Introduction

To minimize the weight of the Thermal Protection System required on the leeside of winged reentry vehicles, an accurate description of leeside flow is required. The inability of ground test facilities to reproduce the high enthalpy, separated flow present during reentry flight conditions, coupled with the prohibitive expense of flight tests, leads to the use of an analytical method—namely Computational Fluid Dynamics (CFD)—to describe the flow.

While the ultimate goal of this work is to accurately predict the leeside flow and its associated thermal environment, an essential first step towards that goal is a comparison of CFD pressure predictions with wind tunnel data. Until such CFD pressure predictions agree with wind tunnel test cases, there is little hope of accurately predicting the thermal environment at flight conditions. Thus, the objective of this study is to compare the pressure distributions predicted by inviscid, perfect gas CFD to Shuttle Orbiter wind tunnel data and to address any significant issues encountered during the computation.

While flight data is available for the Shuttle Orbiter, a wind tunnel case is chosen for this study to allow a tractable problem for preliminary investigation. Using a wind tunnel case allows the perfect gas assumption for the flow chemistry. This provides a significant computational savings over a several species finite-rate chemistry model which would be necessary if high-temperature effects present at flight conditions were to be included. In addition, by concentrating on the surface pressures, the analysis need only consider inviscid flow. This further reduces the computational expense due to the absence of viscous terms and the associated decrease in the number of points required for the computational grid.

One of the first codes applied to a winged reentry vehicle at moderate angles of attack was the STEIN (Supersonic/hypersonic Three-dimensional External Inviscid flow) code of Marconi *et al.*[1] Due to the coordinate transformations employed, the code could treat only relatively simple geometries consisting of a fuselage, a perpendicular wing, and a tail. The code used an elliptic solver for the subsonic nose region coupled with a marching solution for the rest of the vehicle and treated embedded shocks discreetly. As a consequence of the marching procedure, the code could not tolerate embedded subsonic regions such as those on the leading edge of the Shuttle Orbiter's wing at high angles of attack.

A second code, the HALIS (High Alpha Inviscid Solution) code of Weilmuenster,[2] was

created to alleviate the subsonic pocket restrictions of a pure marching scheme like STEIN. The time-asymptotic nature of HALIS modestly increased its memory and computational requirements, but the previous angle of attack restriction was removed. The HALIS code used a combination of spherical coordinates for the nose section and cylindrical coordinates for the fuselage and empennage. This coordinate choice dictated that coordinate lines joining the surface and the bow shock were not permitted to pass through the body surface in the intervening distance. This meant that the Shuttle Orbiter could not be modeled accurately on the leeward side due to the double valued coordinates caused by the wing.

Previous computational efforts (such as STEIN and HALIS) had been directed toward the windward surface quantities, primarily due to restrictions in treating either the winged geometry or its associated subsonic regions at high angle of attack. The code used for this study, the LAURA (Langley Aerothermodynamic Upwind Relaxation Algorithm) code of Gnoffo,[3–5] represents a state-of-the-art code for computing the flow over complex configurations at hypersonic speeds. The code incorporates a curvilinear coordinate system so that arbitrary geometries such as the Shuttle Orbiter can be treated. As with HALIS, the LAURA code casts the governing equations in a time-asymptotic manner, so that embedded subsonic regions are treated implicitly.

In this study, the LAURA code is applied to a wind tunnel condition in order to assess the ability of current CFD methods to predict the flow over a relatively complex hypersonic vehicle at high angles of attack. A brief description of the numerical approach, followed by a discussion of the geometry and associated grid used for this study are presented. Computational results for the Shuttle Orbiter are then compared with wind tunnel data. Additional discussion of numerical difficulties associated with this high angle of attack/delta wing configuration are included.

Approach

Numerical Method

The LAURA code is a point-implicit, finite volume solver based on the upwind-biased flux difference splitting of Roe.[6] The scheme takes advantage of Yee's symmetric total variation diminishing discretization,[7] as well as Harten's entropy fix.[8] The code is capable of

modeling any of three air chemistry assumptions: perfect gas, equilibrium, or thermochemical non-equilibrium. For this study, the code uses the perfect gas, inviscid flow model.

To provide a foundation for later discussion, a brief description of the dissipative nature of Roe's flux difference splitting is necessary. In particular, a first-order accurate representation of a flux, $\mathbf{f}$, across a cell face is given by Eq. 1,

$$\mathbf{f}_{face} = \left[\frac{1}{2}\left(\mathbf{f}_L + \mathbf{f}_R\right) - \left|\mathbf{A}_{face}\right| \frac{1}{2}\left(\mathbf{q}_R - \mathbf{q}_L\right)\right] \tag{1}$$

where $\mathbf{q}$ is the vector of conserved variables at the left ($\mathbf{L}$) and right ($\mathbf{R}$) cell centers and $\mathbf{A}$ is the Roe-averaged flux jacobian. The first term on the right-hand-side of Eq. 1 is a central difference approximation of the flux at the face. This term alone, however, is inherently unstable due to its lack of numerical dissipation. Countering this de-stabilizing effect is the second term which can be thought of as an first order-accurate upwind numerical dissipation. The amount of dissipation is automatically controlled by two things: the "smoothness" of the flow ($\mathbf{q}_R - \mathbf{q}_L \rightarrow 0$) and the magnitude of the eigenvalues of the Roe-averaged flux jacobian ($\mathbf{A}$). When an eigenvalue of $\mathbf{A}$ approaches zero in smooth regions of the flow (*e.g.*, near a sonic line), the artificial dissipation tends to zero. In this situation the eigenvalue limiter of Harten[8] sets a lower bound on the eigenvalue.

For a more detailed description of the numerical algorithm in the LAURA code, see Ref. 5. Descriptions of the physical flow models can be found in Refs. 4 and 9.

Geometry and Computational Mesh

The Shuttle Orbiter vehicle represents a very complex geometric modeling problem, especially the aft portion (see Fig. 1). Since this study is focused on the leeside flow over the vehicle forward of the elevon hinge-line, simplifications are made to the aft section of the vehicle to greatly reduce the analytical geometry modeling and grid generation effort (see Fig. 2). These simplifications are justifiable since the flow in the aft region of the vehicle is predominately supersonic. Thus, the modeling of the geometry aft of the elevon hinge-line has negligible upstream influence. The geometrical simplifications consist of omission of the tail surface, body flaps, and a continuation of the wing's trailing edge thickness as a solid surface extending to the outflow plane. Note, however, that the entire forward portion of the vehicle is accurately modeled.

A database obtained from Johnson Space Center is used to generate a computational surface grid via the GRIDGEN package.[10] The surface grid has 120 points down the body and 140 points circumferential.

The initial volume grid is constructed in two phases. Since the surface grid and an axis of singularity line comprise two of the six volume grid boundary faces, the first phase is to use the GRIDGEN package to generate a surface grid on each of the remaining four boundaries (the upper and lower symmetry planes, the outflow boundary, and the free-stream boundary).

The second phase is to distribute grid points within these boundaries, based on the transfinite grid generation routine of Abolhassani.[11] Trans-finite grid generation, when used to distribute the interior points around a winged-body, has difficulty in the nose and the wing leading edge regions when given only the outermost boundaries. To alleviate these problems, intermediate cross sectional planes are defined to split the entire volume grid into four regions. The method of Ref. 11 is then applied to each region with appropriate matching conditions.

The outer boundaries of the volume grid computed above extend conservatively beyond where the bow shock is estimated to reside. This is necessary since the exact bow shock location and shape is not known a priori and the LAURA algorithm is a shock capturing scheme (*i.e.*, the bow shock must be contained within the computational domain). Therefore, the LAURA algorithm is applied to the initial volume grid for several hundred iterations to determine a more precise position and shape of the bow shock structure, then the grid alignment routine contained within LAURA is called to redistribute the grid points in a more efficient manner. In this study, for example, the initial volume grid had nearly 60 percent of its points outside the bow shock (*i.e.*, in the uniform, free-stream flow); but after the redistribution, the grid had only eight percent of the total points outside the bow shock. The grid alignment routine not only provides better resolution within the shock layer through efficient grid distribution, but also produces grid surfaces which are parallel to the bow shock surface—improving the resolution of the strong bow shock.

The resulting volume grid, which contains just over one million grid points, is shown in Fig. 3. The grid has 120 points along the body, 140 circumferential, and 60 points from the

body to just outside the bow shock.

Results and Observations

Computational results are obtained for flow about the Shuttle Orbiter at $M_\infty = 7.4$ and 40° angle of attack. Free-stream conditions and measured surface pressures are taken from the wind tunnel runs of Dye *et al.*,[12] for which the Reynolds number per foot is 6.5 million. For the CFD conditions, the Reynolds number is infinite since the flow is modeled without viscous terms.

The computational cost of the solution, including the numerical difficulties encountered enroute, the learning curve of the user, and the grid alignment, was nearly 175 Cray-2 hours (running with 70 Megawords of memory). The numerical difficulties encountered during the computational process are discussed below, followed by computed pressure distribution comparisons with measured wind tunnel data.

Numerical Difficulties in the Wing Tip Region

The flow expands around the Shuttle Orbiter's wing tip so that a near-vacuum condition is created on the upper surface. This near vacuum condition causes the numerical scheme within LAURA to fail. The failure is characterized by very sudden departure (within two iterative time-steps) from the nominal convergence rate. The conserved variables indicate that a negative internal energy was computed on the surface just below the wing tip vortex.

A similar failure while using Roe's flux difference splitting was reported by Rausch (private communication, 1991). Rausch was using Roe's flux difference splitting to compute the time-accurate, inviscid flow of a plane shock impinging a cylinder. The scheme would fail just as the triple point was forming on the lee of the cylinder (another near-vacuum region). Rausch found, however, that by switching to van Leer's flux vector splitting[13] the problem could be solved.

Since LAURA algorithm does not have the option of using Van Leer's flux vector splitting, several different approaches were used:

1. increasing the magnitude of Harten's eigenvalue limiter

2. increasing the eigenvalues limiter's dependence on cross-flow velocities

3. decreasing the CFL number

4. redistributing the grid points near the wing tip

5. reducing the grid skewness in the wing tip region

All of the above attempts failed to solve the divergence problem. Usually, these methods simply delayed the onset of the divergence or added so much artificial viscosity that the resulting flow-field was non-physical.

A work-around was accomplished by using the fact that for an inviscid flow, the total enthalpy throughout the flow is the same as the free-stream total enthalpy. Thus, the wall boundary condition was rewritten to enforce free-stream total enthalpy at the wall. Note, however, that this type of fix will not work for a viscous calculation since the total enthalpy is no longer a constant throughout the flow-field. It could be expected, however, that the viscous damping effects might alleviate the problem.

Recently, a more rigorous fix for this problem was given by Einfeldt, *et al.*[14]

Pressure Comparisons

Figure 4 shows a comparison of computed and measured pressure coefficient distributions along the windward and leeward centerlines of the Shuttle Orbiter. A pressure distribution calculated by the HALIS code for the windward portion of a simplified Shuttle Orbiter is also included. As discussed earlier, the aft portion of the vehicle is not modeled accurately past $X/L = 0.9$. This is clearly evident on the windward surface pressures.

From the figure, there is evidence of a geometric discrepancy between the wind tunnel model and the analytic description of the geometry used for CFD. This occurs between 7 and 20 percent of the distance down the body where the wind tunnel data shows consistently higher pressures. Since the wind tunnel Reynolds number is high (6.5×10^6/ft), it can be argued that the viscous interaction can not account for this size of discrepancy. The HALIS solution also shows similar geometrical inconsistencies due to the fact that its geometry is comprised of a sequence of conic sections which are not slope continuous at their junctures. It is interesting to note, however, that even though the geometric models used with LAURA

and HALIS were developed independently and by different means, the solutions are in good agreement with one another.

The windward surface pressure distribution predicted by LAURA around $X/L = 0.82$ is not smooth. This is due to irregularities in the surface geometry definition. These surface irregularities (on the order of a couple of degrees) are large enough to create compression waves, as can be readily seen in the pressure contours of the aft section of the windward symmetry plane (see Fig. 5).

Figure 6 presents the coefficient of pressure distribution as a function of the angle Φ around the body at various cross section stations. The angle Φ is measured from the windward centerline to the leeward centerline plane. The CFD and wind tunnel data compare very well with the exception of the chine areas ($\Phi = 60°$) and the windward centerline ($\Phi = 0°$). As discussed previously, the centerline discrepancy is apparently a geometrical difference between the wind tunnel model and the CFD model. The chine areas agree well until the last cross section ($X/L = 0.6$). At this station, the location of the pressure decrease around the wing is missed by the CFD solution. Since the first three stations agree well, this could be attributed to slight geometric discrepancies between the wind tunnel model and the CFD model at the leading edge of the wing.

Figure 7 shows the coefficient of pressure distribution at various spanwise stations along the wing as a function of the non-dimensionalized chord position. Again, due to geometrical simplifications to the CFD model at the aft of the vehicle, the portion of the solution beyond the elevon hinge line is to be ignored. The computed pressures are within five percent of the wind tunnel data except at two data points on the windward surface of the inboard semi-span station ($2Y/B = 0.4$).

Concluding Remarks

An inviscid solution for the Shuttle Orbiter was computed for a wind tunnel case. The pressures compare well with the wind tunnel data for both the windward and leeward sides. This implies that at least the salient inviscid flow features are being properly modeled. It was also found that a modified boundary condition was necessary to alleviate the inherent instability of Roe's flux difference splitting in the near-vacuum regions of the Shuttle Or-

biter's wing tip vortex. Also, for this inviscid computation, it was shown that slight surface imperfections of the windward surface of the Shuttle Orbiter noticeably contaminated the solution.

Acknowledgments

The authors would like to thank Norma L. Farr, John E. Stewart, and Jimshid S. Abolhassani of Computer Sciences Corporation, Hampton, VA, and Eric L. Everton of NASA Langley Research Center, Hampton, VA, for providing the database used for the Shuttle Orbiter and assistance in generating the volume grid.

The authors would also like to thank Francis A. Greene and Peter A. Gnoffo of the Aerothermodynamics Branch, Space Systems Division, NASA Langley Research Center for their assistance with the LAURA code.

References

[1]F. Marconi, M. Salas, and L. Yaeger, "Development of a Computer Code for Calculating the Steady Super/Hypersonic Inviscid Flow Around Real Configurations," NASA CR–2675, 1976.

[2]K. J. Weilmuenster and H. H. Hamilton, II, "Calculations of Inviscid Flow Over Shuttle-Like Vehicles at High Angles of Attack and Comparisons With Experimental Data," NASA TP–2103, 1983.

[3]P. A. Gnoffo, "Upwind-Biased, Point-Implicit Relaxation Strategies for Viscous, Hypersonic Flows," AIAA Paper 89–1972, 1989.

[4]P. A. Gnoffo, R. N. Gupta, and J. Shinn, "Conservation Equations and Physical Models for Hypersonic Air Flows in Thermal and Chemical Nonequilibrium," NASA TP–2867, 1989.

[5]P. A. Gnoffo, "An Upwind-Biased, Point-Implicit Relaxation Algorithm for Viscous, Compressible Perfect-Gas Flows," NASA TP–2953, February 1990.

[6]P. L. Roe, "Approximate Riemann Solvers, Parameter Vectors, and Difference Schemes," *Journal of Computational Physics*, vol. 43, pp. 357–372, October 1981.

[7]H. C. Yee, "On Symmetric and Upwind TVD Schemes," NASA TM–88325, 1986.

[8]A. Harten, "High Resolution Schemes for Hyperbolic Conservation Laws," *Journal of Computational Physics*, vol. 49, no. 2, pp. 357–393, February 1983.

[9]F. A. Greene, "Viscous Equilibrium Computations Using Program LAURA," AIAA Paper 91–1389, 1991.

[10]J. P. Steinbrenner, J. R. Chawner, and C. L. Fouts, "The GRIDGEN 3D Multiple Block Grid Generation System: Volume I—Final Report," WRDC TR 90–3022, July 1990.

[11]J. S. Abolhassani, I. Sadrehaghighi, R. E. Smith, and S. N. Tiwari, "Application of LaGrangian Blending Functions for Grid Generation Around Airplane Geometries," *Journal of Aircraft*, vol. 27, no. 10, pp. 873–877, October 1990.

[12]W. H. Dye and T. Polek, "Results of Pressure Distribution Tests on a 0.010-Scale Space Shuttle Orbiter (61-0) in the NASA/ARC 3.5-Foot Hypersonic Wind Tunnel (Test OH38)," NASA CR–144584, 1975.

[13]B. van Leer, "Flux Vector Splitting for the Euler Equations," *Lecture Notes in Physics*, vol. 170, pp. 507–512, July 1982.

[14]B. Einfeldt, C. D. Munz, P. L. Roe, and B. Sjögreen, "On Godunov-Type Methods near Low Densities," *Journal of Computational Physics*, vol. 92, pp. 273–295, February 1991.

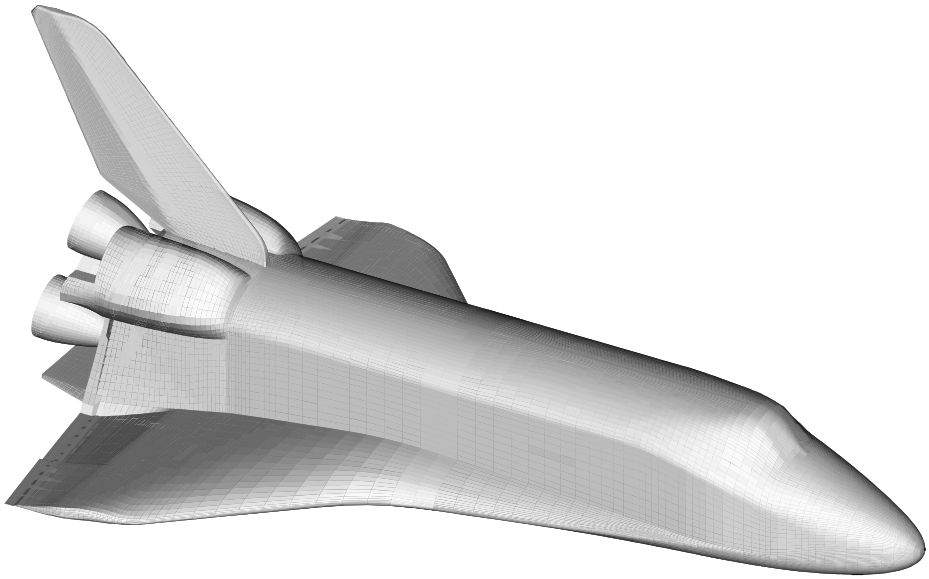

Figure 1: Shuttle Orbiter surface definition.

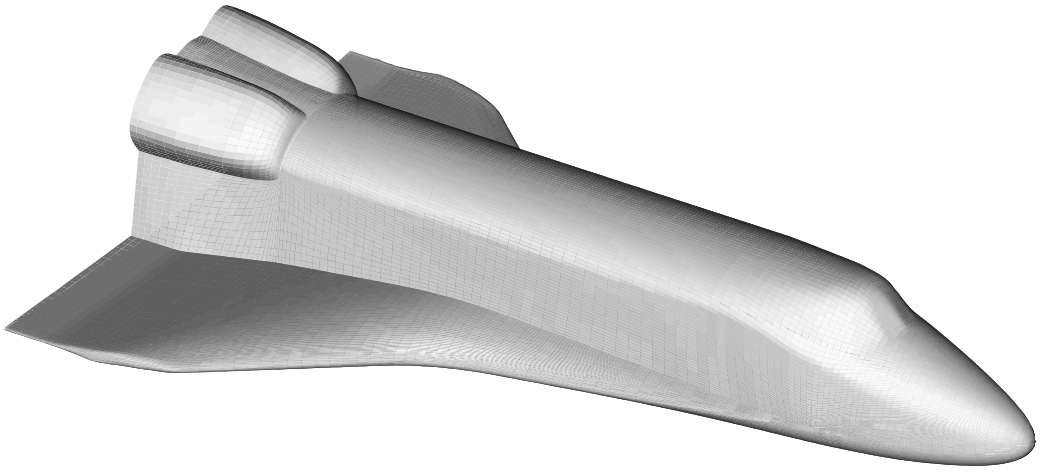

Figure 2: Simplified Shuttle Orbiter surface definition.

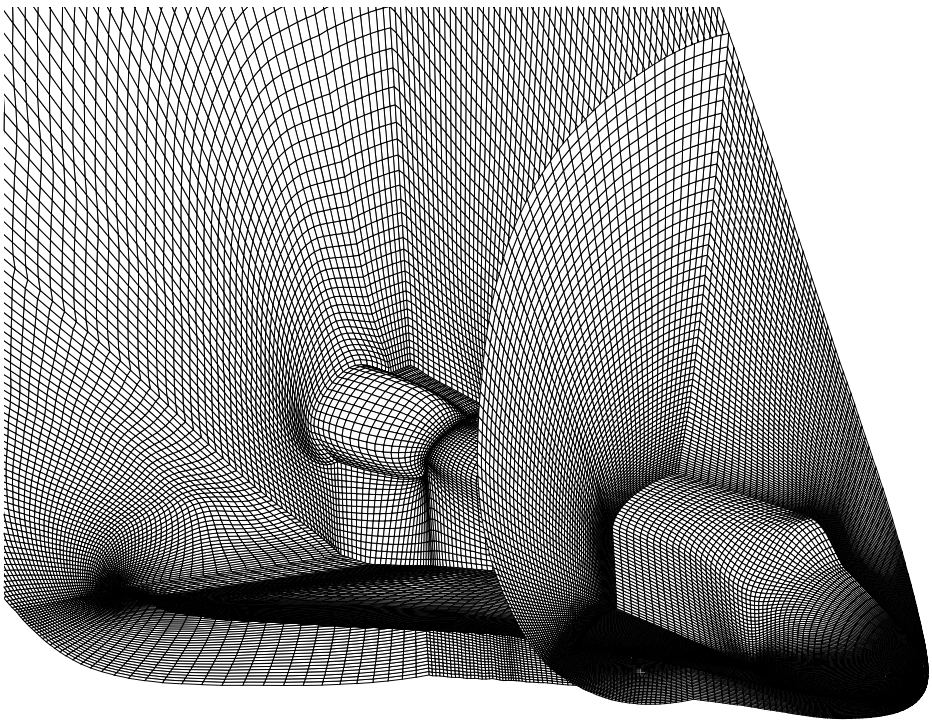

Figure 3: A depiction of the volume grid used for the Shuttle Orbiter computation.

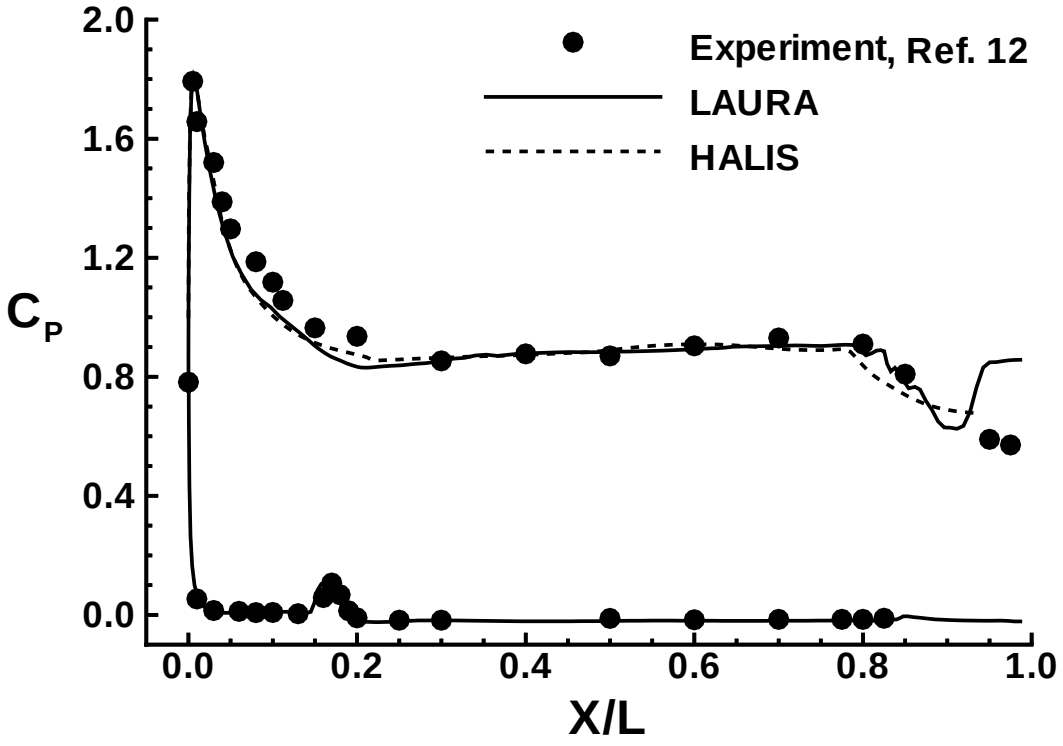

Figure 4: Comparison of pressure coefficient along the windward and leeward centerlines of the Shuttle Orbiter at $M_\infty = 7.4$ and 40° angle of attack.

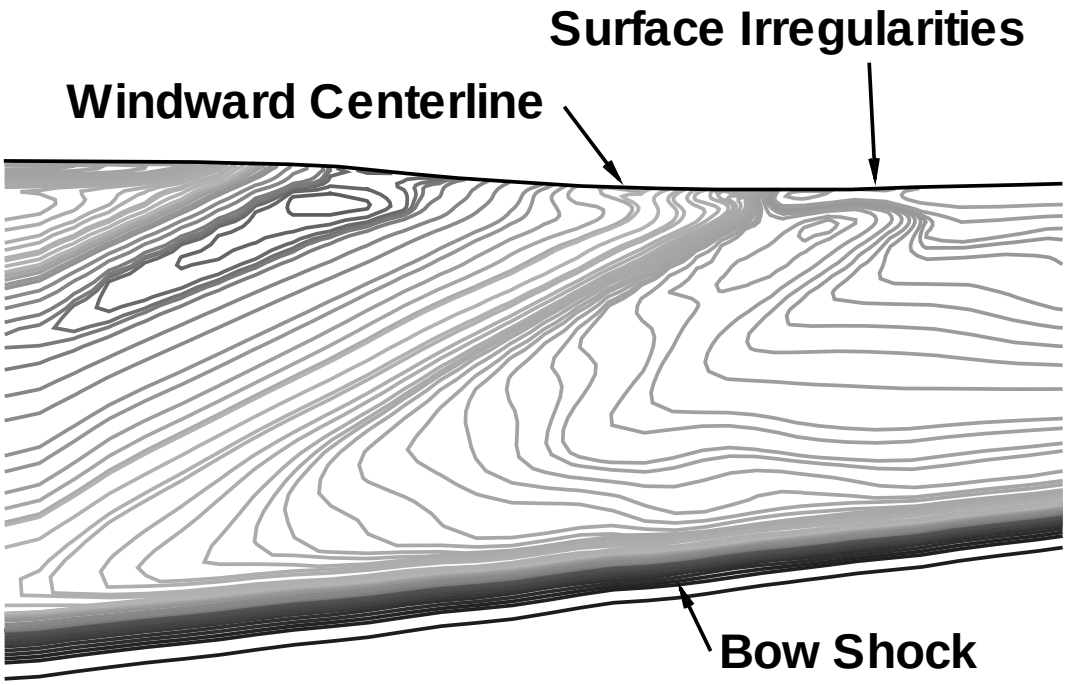

Figure 5: Pressure contours in the aft portion of the windward symmetry plane for the Shuttle Orbiter at $M_\infty = 7.4$ and 40° angle of attack.

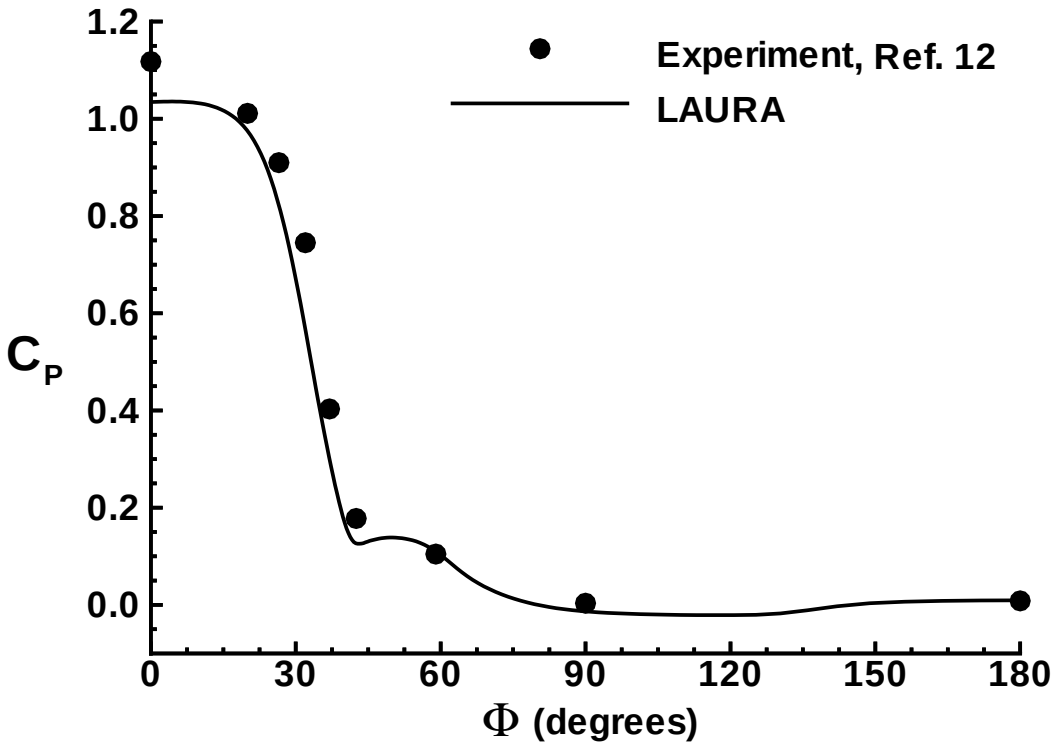

a.) Fuselage station, X/L=0.1

Figure 6: Comparison of pressure coefficient at various fuselage cross sections for the Shuttle Orbiter at $M_\infty = 7.4$ and $40°$ angle of attack.

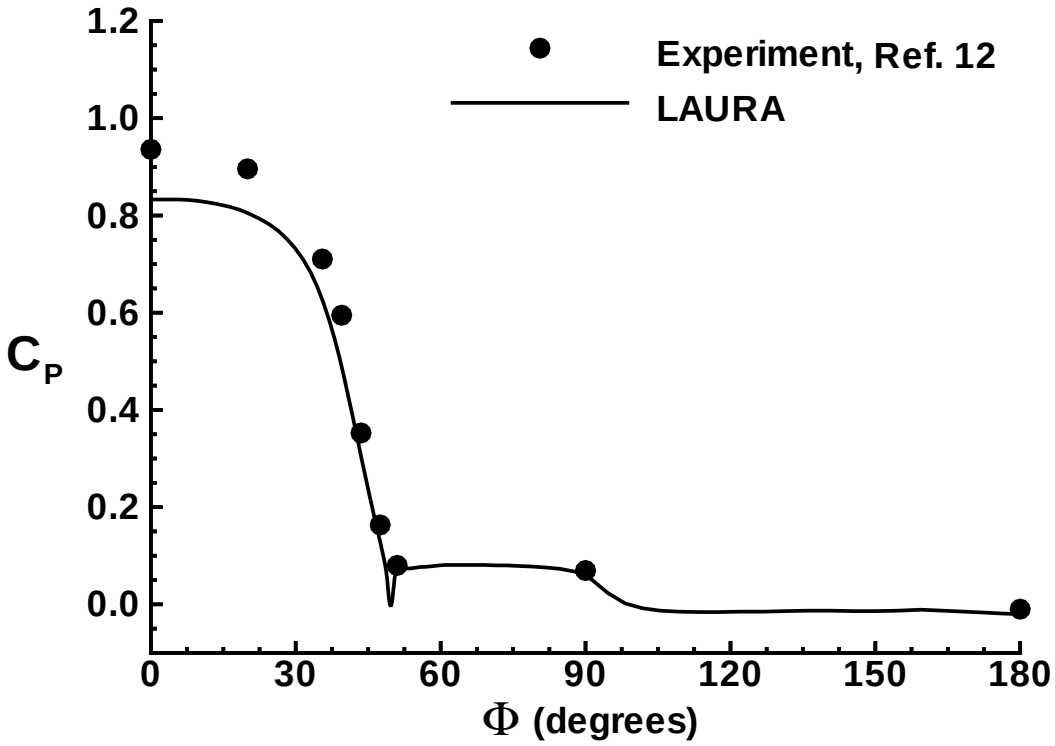

b.) Fuselage station, X/L=0.2

Figure 6: Continued.

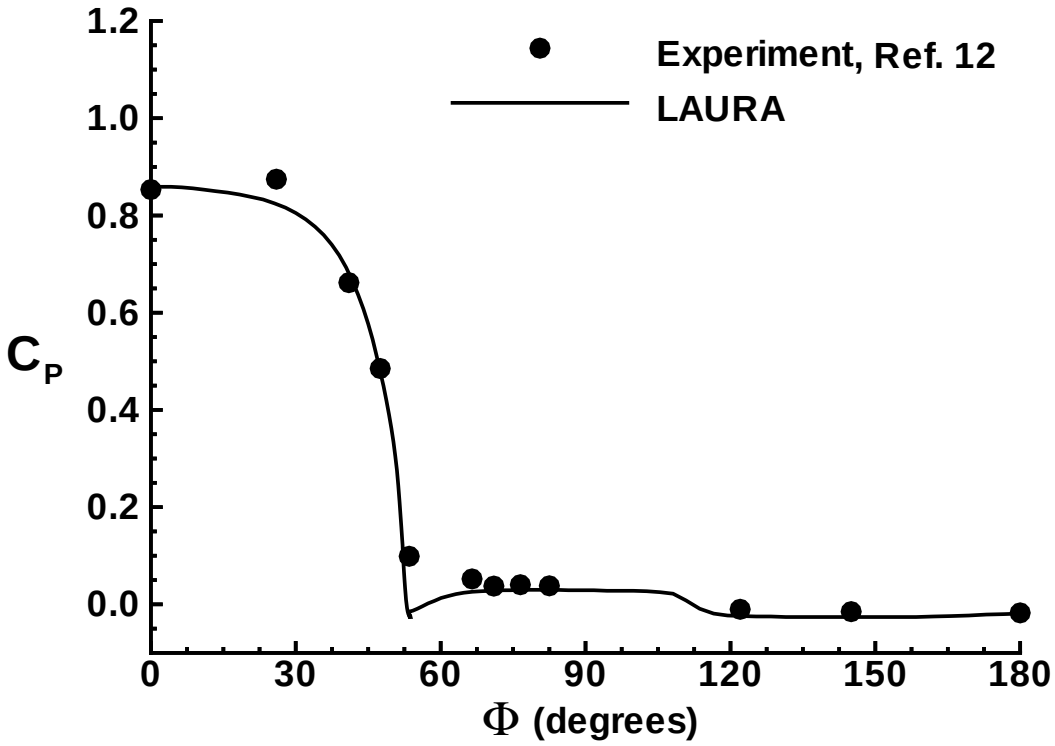

c.) Fuselage station, X/L=0.3

Figure 6: Continued.

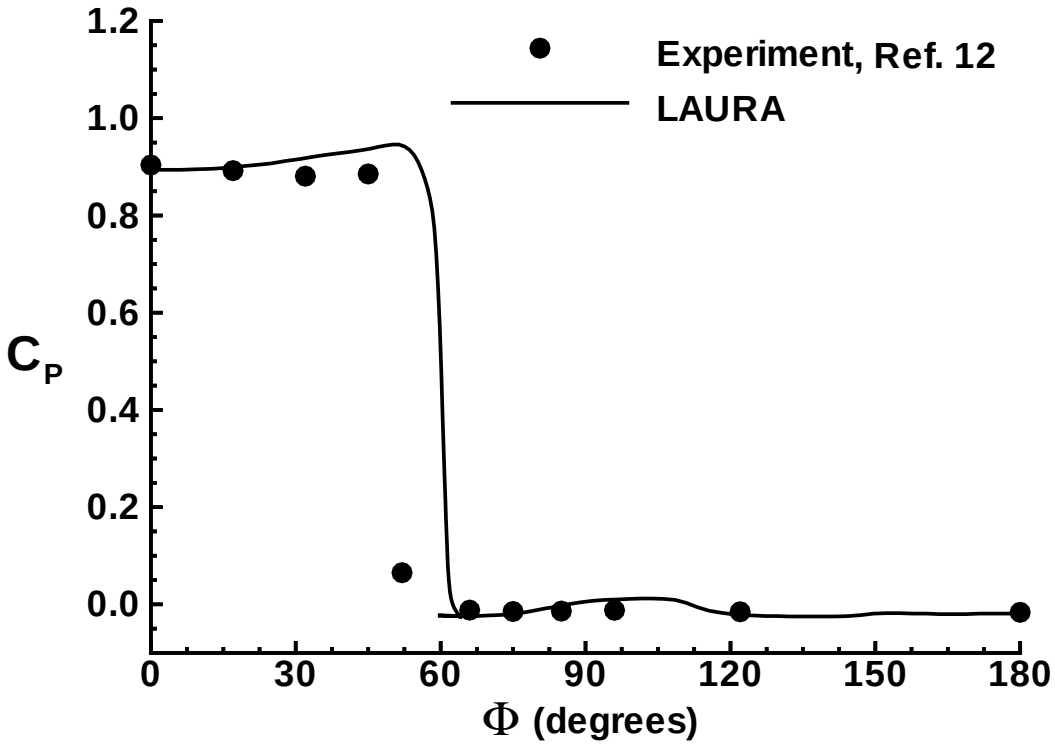

d.) Fuselage station, X/L=0.6

Figure 6: Concluded.

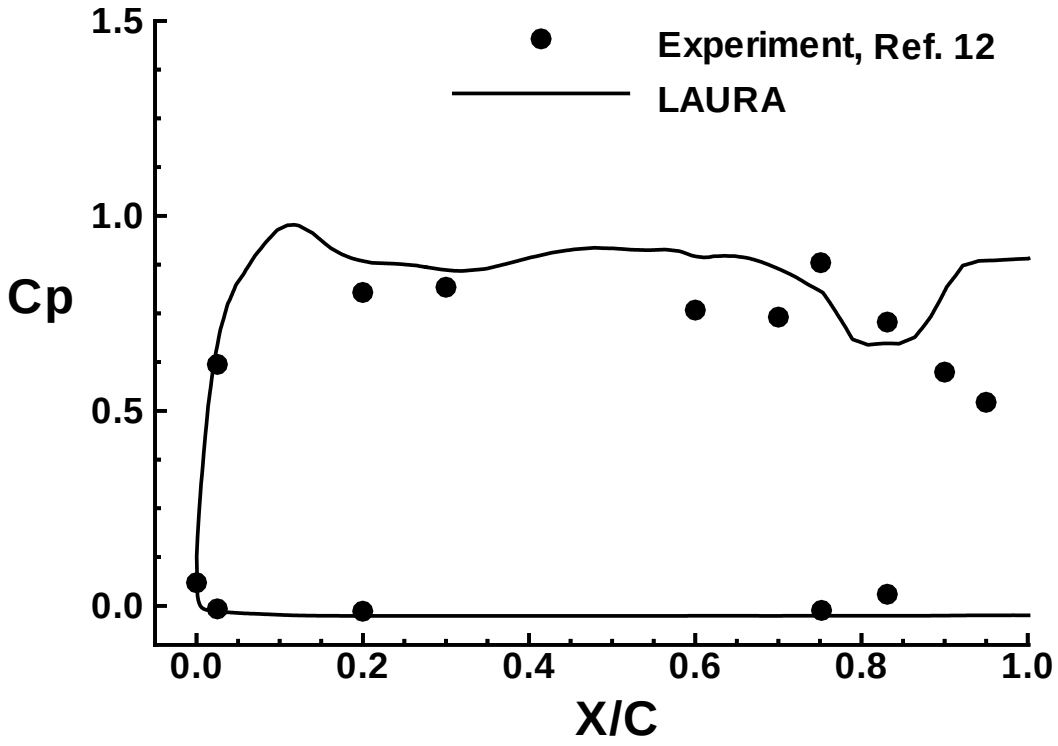

a.) Wing semi-span station, 2Y/B=0.4

Figure 7: Comparison of pressure coefficient at various spanwise stations along the wing as a function of non-dimensionalized chord position for the Shuttle Orbiter at $M_\infty = 7.4$ and 40° angle of attack.

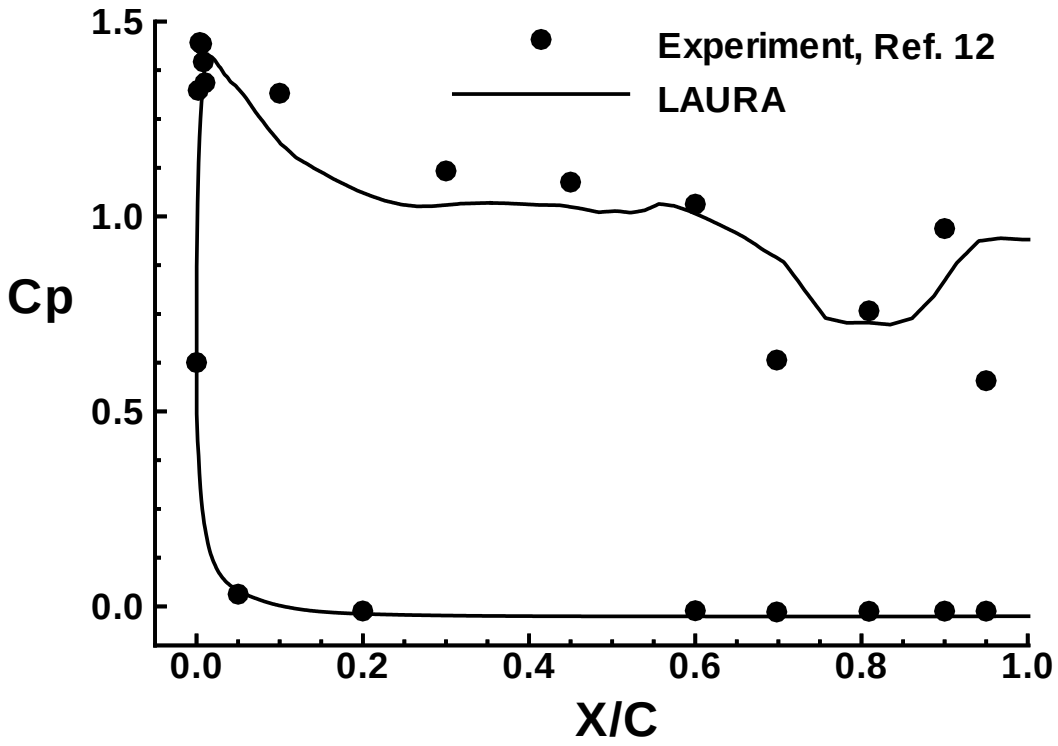

b.) Wing semi-span station, 2Y/B=0.6

Figure 7: Continued.

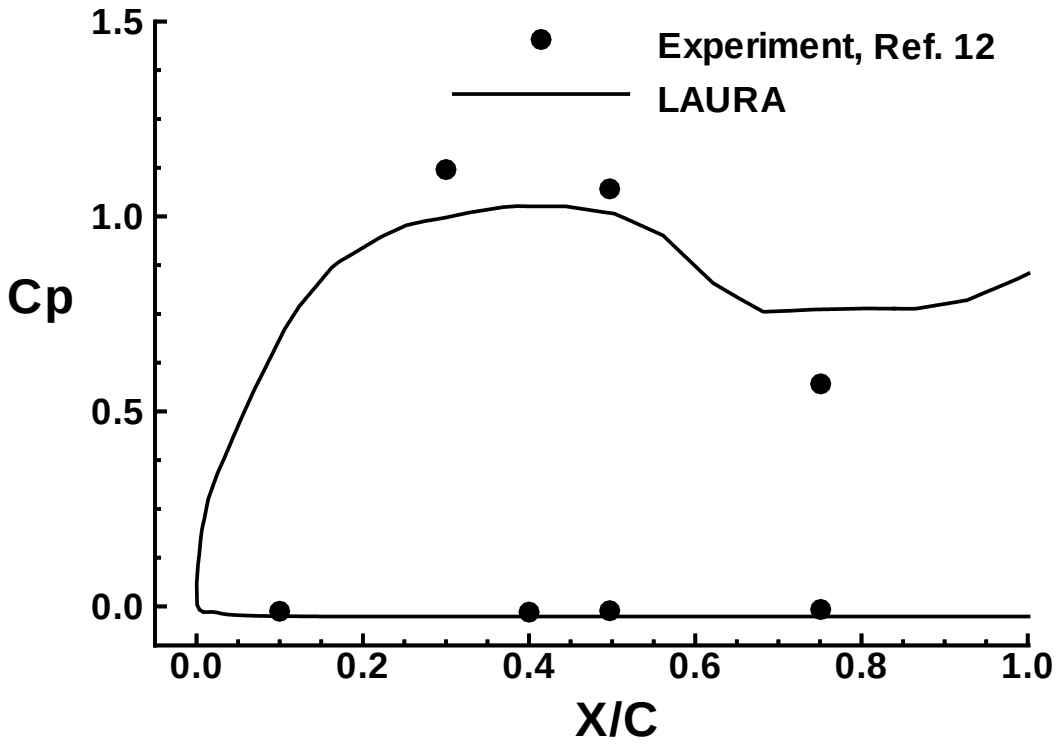

c.) Wing semi-span station, 2Y/B=0.95

Figure 7: Concluded.